CLOUD MASKING USING RED AND NEAR-INFRARED BANDS

Mark Jayson Felix[1] and Dr. Gay Jane Perez[2]
[1,2]Institute of Environmental Science and Meteorology
University of the Philippines Diliman, Quezon City, Philippines
[1]Email: markjaysonfelix@gmail.com
[2]Email: gpperez1@up.edu.ph

KEY WORDS: DIWATA-1, Spaceborne Multispectral Imager, Landsat8-OLI

ABSTRACT: In this work, a simple cloud mask algorithm that only utilizes the red and near-infrared (NIR) bands of a multispectral imager was employed and assessed using daytime Landsat8 dataset. The cloud mask algorithm uses an ancillary land/water mask generated using a threshold applied to the calculated NDVI values. Accuracy assessment using the quality assessment band provided in each Landsat8 dataset shows a good agreement on the computed cloud cover area percentage. Moreover, the red-NIR cloud mask algorithm for each processed Landsat8 dataset achieved an overall accuracy no less than 90%. Further analysis showed undetected cloud pixels by the quality assessment band of Landsat8 dataset which are detected by the red-NIR cloud mask algorithm. This shows the potential efficacy of the red-NIR cloud mask algorithm for satellites without onboard thermal imager such as Philippines' first earth-observation microsatellite named DIWATA-1.

1. INTRODUCTION

DIWATA-1, The Philippines' first earth-observation microsatellite has an onboard Spaceborne Multispectral Imager (SMI) which can take images from different bands ranging from blue (440 nm) to NIR (1000 nm). The SMI can provide important information that may be used for assessing vegetation health and ocean productivity in a large scale. However, accurate earth-observation and analysis for such applications may be contaminated by the presence of clouds. Hence, identification of cloud pixels is of high importance to avoid erroneous analysis of satellite images. Conventionally, cloud mask algorithms utilize visible, NIR, SWIR and thermal band images (4 and 11 µm) to differentiate cloud pixel from other satellite image pixels classified as land, vegetation, desert and water (Ackerman, 1997) (Frey, 2008) (Chylek, 2006). This is based on the temperature difference of clouds among others (except snow) with clouds having cooler temperature. Additionally, a land/water mask is used as an ancillary data on cloud mask algorithms since different thresholds are applied for land and water pixels. However, DIWATA-1 has no onboard thermal imager and SWIR, hence conventional cloud mask algorithms that utilized thermal bands cannot be used.

Cloud mask algorithms based on NIR and short-wave infrared (SWIR) have been developed (Nordkvist, 2009) (Martins, 2002) (Simpson, 1998). However, these algorithms are specific for vegetation or water bodies only. In this work, a simple cloud mask algorithm for land areas and water bodies that only utilizes the red and NIR bands was employed. Furthermore, a Normalized-Difference Vegetation Index (NDVI)-based land/water mask was used on the proposed red-NIR cloud mask algorithm. An NDVI-based land/water mask has the advantage of having a spatial resolution similar to the native resolution of the satellite image to be processed. Unlike other known land/water masks that have a fixed spatial resolution, the proposed land/water mask adapts to the spatial resolution of the image removing the need for resampling which introduces additional step on the data processing and analysis. Furthermore, with a spatial resolution of 30m, the generated land/water mask was able to distinguish inland waters and water ways. The cloud mask algorithm is initially tested on LandSat8-OLI images captured within the Philippine area. Accuracy assessment of the red-NIR cloud mask algorithm was conducted using the accompanying Quality Assessment band of the Landsat8 dataset.

2. METHODOLOGY

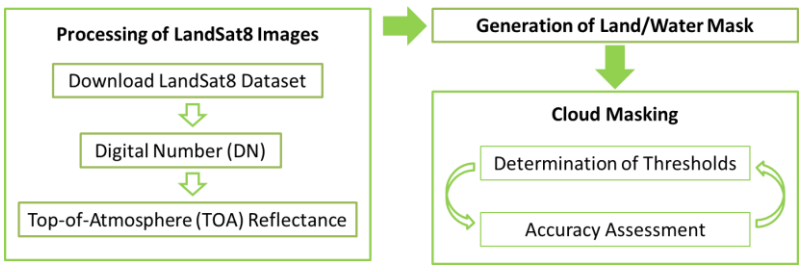

Figure 1. The general workflow for the cloud mask algorithm

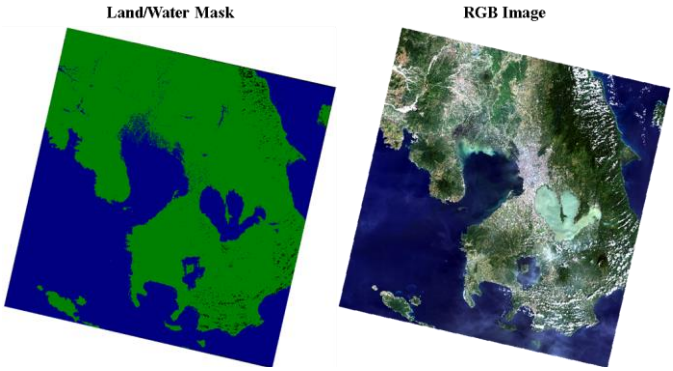

Figure 2. Shows the generated land/water mask derived from the NDVI values.

The workflow of the proposed Red-NIR cloud mask algorithm is shown in Figure 1. The workflow is divided in three subgroups: i) processing of the Landsat8 dataset, ii) generation of land/water mask and iii) cloud masking. First, Landsat8 images taken on Philippine area were downloaded and processed to retrieve the TOA reflectance using the information provided in the metadata file. The TOA reflectance is given by equation 1,

$$TOA_{refl} = \frac{(F_{multiply} \cdot \mathrm{DN}) + F_{add}}{\sin\theta} \tag{1}$$

where $F_{multiply}$ is the multiplicative factor, F_{add} is the additive factor and θ is the sun elevation angle. Subsequently, the land/water mask is generated using the information provided from the calculated NDVI (Zanter, 2015). The NDVI is given by equation 2,

$$NDVI = \frac{NIR_{TOA} - Red_{TOA}}{NIR_{TOA} + Red_{TOA}} \tag{2}$$

where NIR_{TOA} and Red_{TOA} are the calculated TOA reflectance using bands 5 (851-879 nm) and 4 (636-673 nm) of Landsat8 dataset respectively. Using the threshold technique, pixel values with $NDVI \geq 0.05$ are flagged as land otherwise pixels are flagged as water body (Bhandari, 2012) (Rokni, 2014). However, this threshold flags pixels covered by relatively thick clouds as water body. Hence additional threshold was applied to flag these pixels; thick clouds with unknown classification if $NDVI \leq 0.05$ and $Red_{TOA} \geq 0.35$. The generated land/water mask for a test Landsat8 data is shown in Figure 2. It can be observed that inland waters and water ways are distinguishable from the generated land/water mask. The actual cloud masking process is separated in two parts: i) determination of the thresholds and ii) accuracy assessment. For the determination of thresholds, the reflectance properties of different classification such land areas which include vegetation and soil, water bodies, and clouds were analyzed using their corresponding histogram shown in Figure 3. It can be seen that clear land pixels have red and NIR reflectance ranging from 0 – 0.2 and 0 – 0.5 respectively. For clear water pixels, the red and NIR reflectance range from 0 – 0.04 and 0 – 0.02. Offhand, cloud pixels have red and NIR reflectance greater than 0.18 and 0.3 respectively. The histogram analysis was also conducted on images with different sun elevation; a parameter that affects the TOA reflectance. From the histogram analysis of different classifications and images with different sun angle, the determined thresholds are as follow:

For **Land**: cloud pixel if $Red_{TOA} \geq 0.11 * C(\theta)$ and $NIR_{TOA} \geq 0.12 * C(\theta)$
For **Water**: cloud pixel if $Red_{TOA} \geq 0.07 * C(\theta)$ and $NIR_{TOA} \geq 0.08 * C(\theta)$

where $C(\theta)$ is a factor dependent on the sun elevation angle. Lastly, accuracy assessment was conducted using the accompanying Quality Assessment band (BQA) of Landsat8 dataset. The performance of the Red-NIR cloud mask algorithm was assessed via calculation of the missed cloud pixel (%), false detection (%) and overall accuracy (5%) defined by equations 3, 4 and 5 respectively. Note that only pixels with high confidence cloud remark in the BQA was used to extract the reference cloud mask product.

$$\%\, Missed = \frac{\text{number of missed cloud pixels}}{\text{total number of cloud pixels}} \tag{3}$$

$$\%\, False = \frac{\text{number of clear pixels falsely detected as cloud pixels}}{\text{total number of clear pixels}} \tag{4}$$

$$\%\, Accuracy = \frac{\text{number of corect detection}}{\text{total number of pixels}} \tag{5}$$

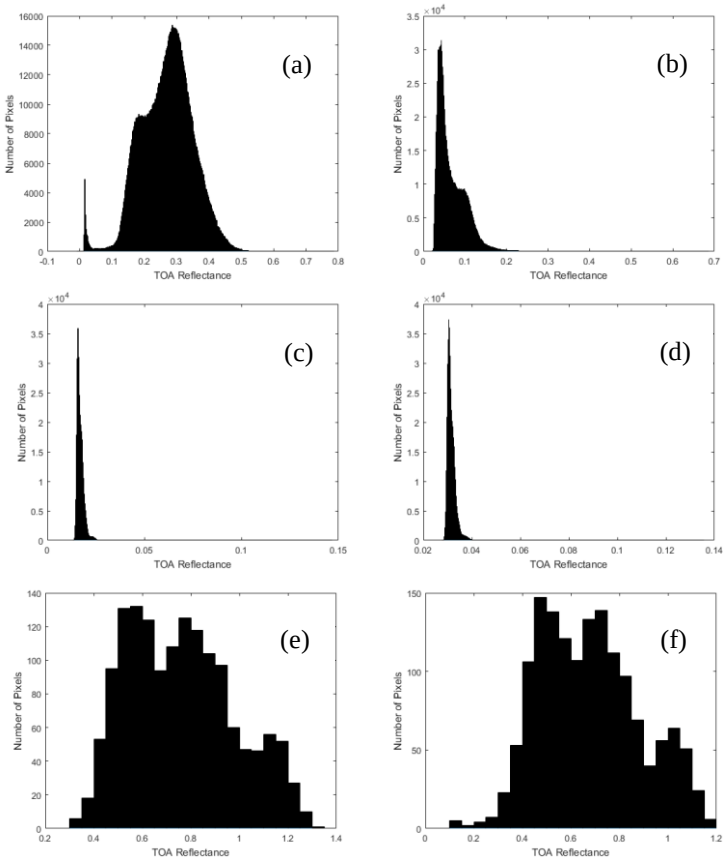

Figure 3. Histogram of a) clear land pixels in NIR_{TOA} band b) clear land pixels in Red_{TOA} band c) clear water pixels in NIR_{TOA} band d) clear water pixels in Red_{TOA} band e) cloud pixels in NIR_{TOA} band and f) cloud pixels in Red_{TOA} band

3. RESULTS & DISCUSSION

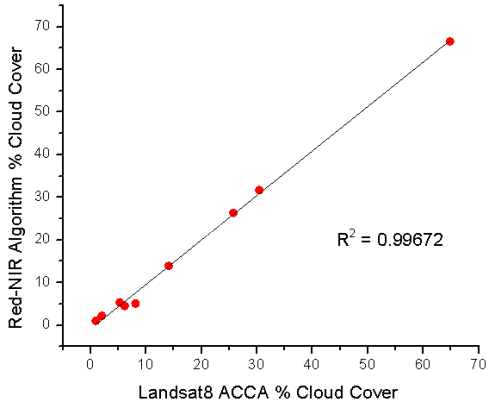

Figure 4. Correlation of the cloud cover percentages computed by the Landsat8 Automated Cloud Cover Assessment Algorithm (ACCA) and red-NIR cloud mask algorithm

A comparison of the computed cloud cover percentage by Landat8 ACCA and red-NIR cloud mask algorithm is shown in Figure 4. A good linear correlation between the Landsat8 ACCA and red-NIR cloud mask algorithm computed cloud cover area percentage with an R^2 of 0.99672 was achieved. This shows the efficacy of a simple cloud mask algorithm without utilizing the thermal bands conventionally used in cloud mask algorithms. The difference on the calculated cloud cover area percentage may be due to several factors such false detection of the red-NIR cloud mask algorithm in urban areas where reflectance in NIR and red is relatively high. Moreover, thin clouds detected by the Landsat8 BQA are possibly missed on the current algorithm. To further evaluate the performance of the red-NIR cloud mask algorithm, the accuracy (%), missed cloud pixel (%), and falsely detected cloud pixels (%) for every test Landsat8 dataset are shown in Table 1. It can be observed that the datasets with highest accuracy (%) are those with lowest false detection (%) and cloud cover difference. Offhand, the datasets with the highest missed cloud pixels (%)

have the highest cloud cover difference. Furthermore, the accuracy (%) drops with increased cloud cover area. In this work, it was observed that reducing the false detection (%) rather than reducing the missed cloud pixel results to higher accuracy. Reduction of the missed cloud pixel consequently results to lower threshold which may directly increase the number of false detection. In a typical image with cloud cover area of 0 – 30%, lower thresholds may result to higher number of incorrect detection due to falsely flagged cloud pixels on the remaining 70-100% clear pixels compared to missing some of cloud pixels in the 0-30% cloud cover thus explains higher accuracy by reducing false detection rather than missed cloud pixels. Figure 5 shows the comparison of the output cloud masks using the red-NIR algorithm and Landsat8's quality assessment band.

However, it should be noted that the band quality assessment (BQA) incorporated in every Landsat8 dataset has an accuracy no greater than 88%. Hence, incorrect detection of cloud and clear pixels by Landsat8's BQA is possible. An example of this is shown in Figure 6. Further image analysis showed some undetected cloud pixels (encircled area) using the BQA of Landsat8 which are flagged as clouds by the red-NIR cloud mask algorithm. This shows a simple, fast and relatively accurate cloud mask algorithm that can be adapted to other multispectral earth-observation satellite. However, the employed cloud mask algorithm is limited to daytime images without the presence of snow.

Table 1. Shows the statistics on the missed cloud pixels, false detection, and accuracy per Landsat8 dataset analyzed in this work

Landsat8 Data	Landsat8 Cloud Cover (%)	Red-NIR Cloud Cover (%)	|CC Difference|	Missed Cloud Pixels (%)	False Detection (%)	Accuracy (%)
LC81160512016076[c]	5.279	5.344	0.065	7.550	0.489	99.138
LC81150502014159[a]	25.757	26.342	0.585	4.759	2.439	96.964
LC81150542016005	6.173	4.477	1.695	18.290	0.079	98.088
LC81160502016044[b]	2.033	2.208	0.175	12.989	0.448	99.297
LC81160502016076	14.090	13.915	0.175	8.621	1.210	97.746
LC81160522016044	0.973	1.050	0.077	12.283	0.198	99.684
LC81170522016051	8.115	5.087	3.028	37.762	0.040	96.899
LC81130522016215	30.427	31.686	1.259	12.187	7.139	91.325
LC81150512016229	64.843	66.548	1.705	5.618	15.211	91.009

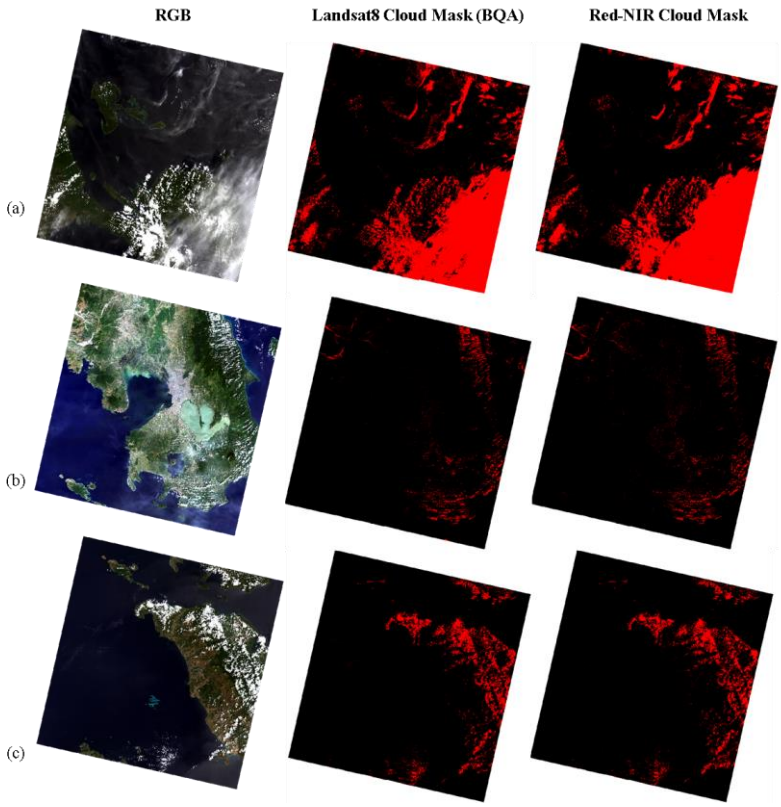

Figure 5. Shows the RGB, Landsat8 BQA and Red-NIR cloud mask images of a) LC81150502014159 b) LC81160502016044 and c) LC81160512016076 dataset

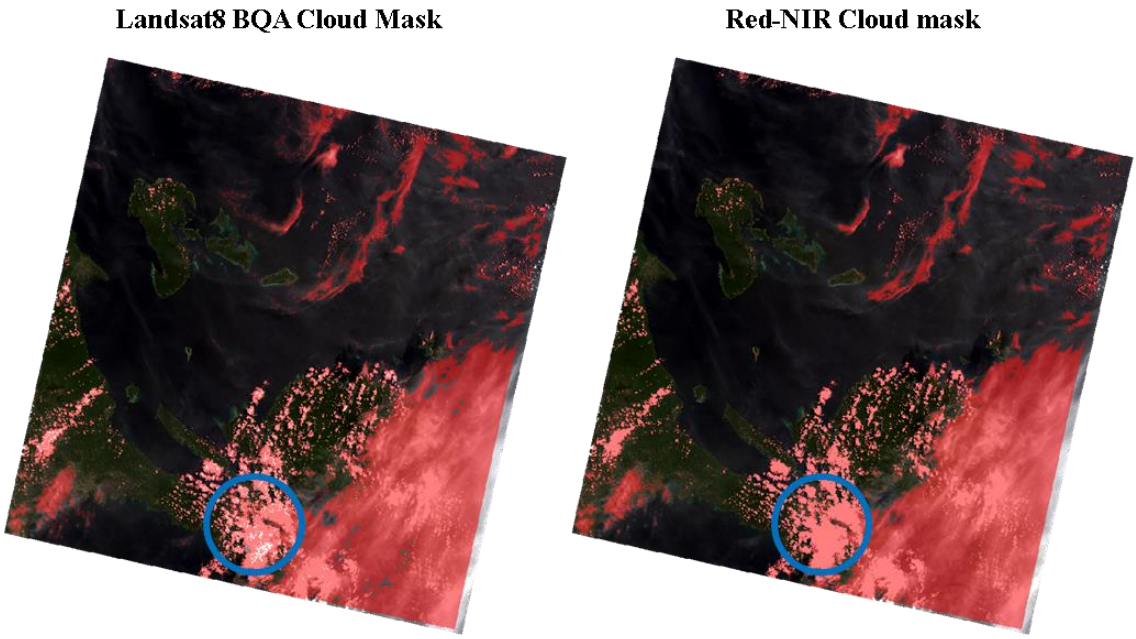

Figure 6. Shows the RGB image with overlaid cloud mask extracted from Landsat8's BQA and Red-NIR algorithm.

4. CONCLUSION

This study was able to demonstrate a simple, fast and relatively accurate cloud mask algorithm (with an overall accuracy more than 90%) that can be adapted to other multispectral earth-observation satellite. Moreover, inland waters and water ways are distinguished from the generated land/water mask which may be useful on simultaneous analysis of vegetation and inland waters such as lakes and estuaries. However, the current employed cloud mask algorithm is limited to daytime images and tropics area where snow is absent. Furthermore, cloud shadows are not evaluated.

5. ACKNOWLEDGMENTS

This research is supported by the Philippine Council for Industry, Energy and Emerging Technology Research and Development (PCIEERD) of the Department of Science and Technology (DOST) through the project Remote Sensing Product Development (PHL MICROSAT Project 5).

6. REFERENCES

Ackerman, S., 1997. DICRIMINATING CLEAR-SKY FROM CLOUD WITH MODIS ALGORITHM TEORETICAL BASIS DOCUMENT (MOD35), version 3.2, pp. 1-100

Bhandari, A.K., 2012. Feature Extraction using Normalized Difference Vegetation Index (NDVI): a Case Study of Jabalpur City, 2nd International Conference on Communication, Computing & Security [ICCCS-2012], Procedia Technology, Vol. 6, pp. 612-619

Chylek, P., 2006. Comparison of near-infrared and thermal infrared cloud phase detections, Journal of Geophysical, Vol.111, pp. 612-619

Frey, R.A., 2008. Cloud Detection with MODIS. Part I: Improvements in the MODIS Cloud Mask for Collection 5, Journal of Atmospheric and Oceanic Technology, Vol. 25, pp. 1057-1072

Martins, J.V., 2002. MODIS Cloud Screening for Remote Sensing of Aerosols over Oceans Using Spatial Variability, Geophysical Researcher Letters, Vol. 29, pp. 1-4

Nordkvist, K., 2009. Cloud Masking of SeaWiFS Images over Coastal Waters Using Spectral Variability, Optics Express, Vol. 17, pp. 12246–12258

Rokni, K., 2014. Water Feature Extraction and Change Detection Using Multitemporal Landsat Imagery, Remote Sensing, Vol. 6, pp. 4173-4188

Simpson, J.J., 1998. A procedure for the Detection and Removal of Cloud Shadow from AVHRR Data over Land, IEEE Transactions on Geoscience and Remote Sensing, Vol. 36, pp. 880-895

Zanter, K., 2015, LANDSAT 8 (L8) USERS HANDBOOK, version 1.0, Department of the Interior U.S. Geological Survey, pp. 46-65